JOURNAL OF MATERIALS SCIENCE 23 (1988) 4157–4164

Dielectric properties of (Ba, Nb) doped TiO_2 ceramics: Migration mechanism and roles of (Ba, Nb)

JENN-MING WU, CHI-JEN CHEN
Department of Materials Science and Engineering, National Tsing Hua University, Hsinchu, Taiwan 30043

Ultrahigh relative dielectric constants with stable frequency and temperature dependence as well as relatively low loss tangent are found in barium and niobium doped TiO_2 ceramics with a silver electrode. The roles of barium and niobium on the dielectric properties of the ceramics are explained after the migration mechanism and the influence of barium and niobium have been analysed. Both silver electrodes made from silver paste and evaporated aluminium electrodes are employed in the study, their effects are also discussed. The migration mechanism proposed is electron hopping among oxygen vacancies. Dissolving barium into TiO_2 ceramics creates an additional oxygen vacancy which results in an increase in conductivity and relaxation frequency of the loss tangent. In contrast, niobium tends to reduce the concentration of oxygen vacancies and causes the opposite effect. The effects of barium and niobium on the concentration of the oxygen vacancy are supported by results of densification and microstructural investigations.

1. Introduction

Space charge polarization usually produces very high dielectric capacitance in materials such as boundary segregated ceramics. Koops [1] derived equations to explain the dispersion of dielectric properties of nickel zinc ferrite ceramics. The equations imply that the following requirements should be met to obtain high dielectric capacitance: (a) r_1 (resistivity of grain boundary layer) $\gg r_2$ (resistivity of grain); (b) x (the ratio of thickness of grain boundary layer to grain diameter) $\ll 1$; and (c) $xr_1/r_2 \simeq 1$.

Yan and Rhodes [2] succeeded in preparing ceramics with ultrahigh dielectric capacitance by doping TiO_2 with barium and tantallum (or niobium). It is believed that tantallum (or niobium), with almost the same size as titanium dissolves easily into the TiO_2 grain and provides one electron which causes the resistivity of the grain to decrease. In contrast, barium, with a much larger size than titanium, tends to segregate in the boundary region and traps two electrons which increases the resistivity of the boundary segregation layer. This explains the resulting ultrahigh dielectric capacitance of the TiO_2 ceramics. However, the resistivities of barium and niobium doped TiO_2 ceramics were not carefully analysed and the effects of niobium (or tantallum) and barium on the resistivities were not discussed in depth. The objectives of this investigation are to characterize related dielectric mechanisms of barium and niobium doped TiO_2 ceramics and to determine the function of barium and niobium on the dielectric properties and conductivities of TiO_2 ceramics.

2. Activation energy of migration mechanism

Dispersion of the dielectric constant is usually observed in the low frequency region for boundary segregated ceramics. This is caused by different resistivities between the grain boundary layer and the grain. Maxwell [3] and Wagner [4] derived equations to describe the phenomenon under the assumption that the resistivity of the grain boundary layer is much larger than that of the grain. According to their derivations, the loss tangent is expressed as

$$\tan \delta = \frac{K\omega t}{1 + K + \omega^2 t^2} \tag{1}$$

where

$$K = \frac{9vk_1}{2k_1 + k_2}$$

$$t = \frac{(2k_1 + k_2)}{4\pi\varepsilon_0} r_2$$

where k_1 and k_2 are the relative dielectric constants of the grain boundary layer and the grain, respectively; ε_0 the dielectric permittivity of a vacuum, v is the volume fraction of grain, and ω is the angular frequency. The loss tangent shows a maximum value at relaxation frequency f_r, which can be given as

$$f_r = \frac{\omega_r}{2\pi} = \frac{(1 + K)^{1/2}}{2\pi t} = \frac{2(1 + K)^{1/2}\varepsilon_0}{(2k_1 + k_2)r_2} = \frac{\text{constant}}{r_2} \tag{2}$$

0022–2461/88 $03.00 + .12

TABLE I Compositions of barium and niobium doped TiO_2 ceramics

Composition (mol %)	Sample					
	25IN	25IN20IB	25IN80IB	25IN100IB	25IN120IB	100IN80IB
Nb	0.25	0.25	0.25	0.25	0.25	1.00
Ba	0	0.20	0.80	1.00	1.20	0.80
Ti	100	100	100	100	100	100

The relaxation frequency is inversely proportional to the resistivity of the grain. Koops [1] also derived equations to explain the phenomenon. Although Koops' equations are much more complex, a similar relationship between f_r and r_2 can be obtained after suitable assumptions. Thus by plotting ln (f_r) against $1/T$, the slope of the line is directly related to the activation energy of the migration mechanism which occurs in grains.

3. Experimental procedure

TiO_2 powders doped with barium and niobium were prepared from reagent grade chemicals like $TiCl_4$, $NbCl_5$ and $BaCl_2$. $TiCl_4$ liquid was gradually dripped into deionized water. The temperature of the deionized water was about 4° C, and the volume of the deionized water used was five times that of the $TiCl_4$ liquid. A white turbid solution was formed after mixing $TiCl_4$ with deionized water. Storage in a refrigerator kept at about 4° C for 24 h, caused the $TiCl_4$ aqueous solution to become clear. A $NbCl_5$ aqueous solution was made by dissolving $NbCl_5$ in a 35% HCl solution and then diluting with deionized water; a $BaCl_2$ solution was also prepared by adding $BaCl_2$ into deionized water and stirring to complete dissolution. The prepared $TiCl_4$, $NbCl_5$ and $BaCl_2$ solutions were mixed together in desirable ratios in a beaker. Then, the mixed solution was slowly dripped into a 0.1 M aqueous solution of $(NH_4)_2CO_3$, which was adjusted with NH_4OH to pH = 9.5, to coprecipitate powders containing titanium, barium and niobium. The pH value of the coprecipitating solution was kept at 9.5 by adding suitable NH_4OH solution slowly into the reaction beaker during the coprecipitation process. After the reaction was completed, the coprecipitated powder was filtered and washed with deionized water three times, followed by washing with 99.5% ethyl alcohol and filtering twice. The washed powder was dried with an infrared lamp and then calcined at 950° C for 1 h. After calcination, the powder was ball-milled with ZrO_2 balls in deionized water in a plastic jar for 3 h. 1.5 wt % PVA as well as 1.0 wt % stearic acid were added and ball-milled together with ceramic powders. After ball-milling, the powder was dried, pulverized, and forced to pass #120 sieve for granulation. The granulated powder was then dry pressed at 175 MPa to form pellets of 1.5 cm in diameter and 2 mm in thickness. The pellets were sintered at 1350° C for 2 h in air, and then cooled in furnace.

After sintering, the sintered bulk densities were measured by Archimedes method; the microstructure of the sintered pellets were examined with scanning electron microscope and optical microscope; the crystalline phases were determined by X-ray diffraction. For dielectric properties measurement, two types of electrodes were prepared on sample pellets. Silver electrodes were made on both surfaces of the sintered pellets by coating silver paste on pellet surfaces, baking at 300° C for 5 min, soaking at 550° C for 15 min, and cooling in furnace. Aluminium electrodes were vacuum evaporated on both pellet surfaces. The relative dielectric constant and loss tangent were measured with an LCR meter (Cheng-Hua) in the frequency range from 10 to 10^5 Hz. In order to determine the activation energy of the migration mechanism, the dielectric properties were measured over the temperature range from −25 to 100° C. The compositions of powders prepared are listed in Table I. The impurities were analysed by inductively coupled plasma atomic emission spectroscopy (ICP-AES).

4. Results and discussion

The results of ICP-AES analysis assured us that the concentrations of the major elements such as titanium, barium and niobium were essentially the same as those we started with. As for the minor impurities, their concentrations were listed in Table II, where it is seen that the concentrations of representative impurities are reasonably low, therefore, they should not cause problems.

4.1. The effect of electrodes

The work functions of silver and aluminium metals are almost the same, their application as contact materials on n-type TiO_2 semiconducting ceramics should function similarly. However, the silver electrodes used in this investigation are made from silver paste which contains some low-melting glass to facilitate bonding, an interfacial layer produced by interaction of low-melting glass, silver, and TiO_2 ceramics is expected. If the segregation layer which is thought build up near the grain boundary retards electrons crossing effectively, both electrodes should behave similarly. However, if this is not the case the existence of the interfacial layer may make the silver electrode behave differently from the aluminium electrode. Fig. 1a shows the frequency dependence of the loss tangent of samples with an aluminium electrode, illustrating

TABLE II Representative impurity concentrations in barium and niobium doped TiO_2 powders as determined by (ICP-AES)

Element	Amount (p.p.m.)	Element	Amount (p.p.m.)
Al	< 30	Mn	< 20
B	< 80	Mo	< 50
Ca	< 30	Si	200–400
Cd	< 10	Na	< 50
Cr	< 50	Ni	< 30
Cu	< 50	Zn	< 40
Fe	< 20	Zr	< 50
Mg	< 10		

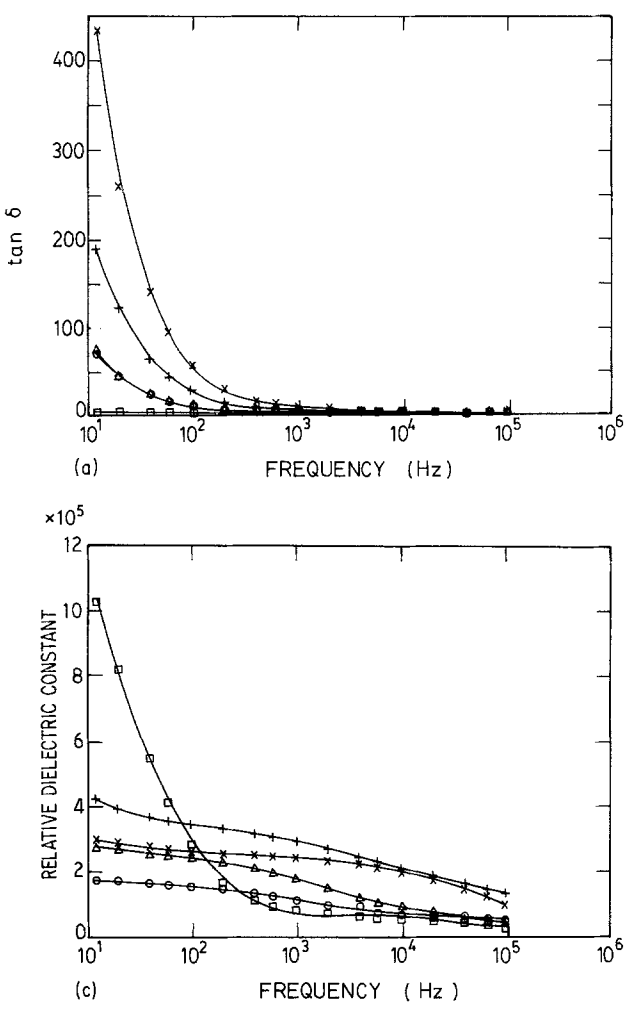

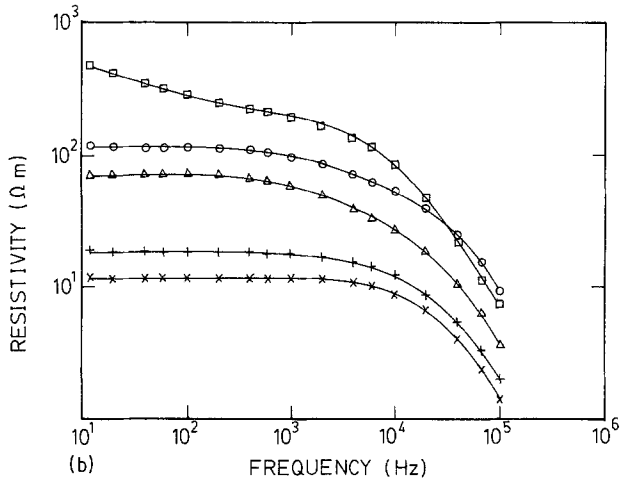

Figure 1 Frequency dependence of (a) tan δ, (b) resistivity, and (c) relative dielectric constant for samples with aluminium electrode. Sinter at 1350° C. (□ 25IN (1450° C), ○ 25IN20IB, △ 25IN80IB, +25IN100IB, × 25IN120IB).

that the loss tangent is very high in the low frequency region and decreases rapidly with frequency. Fig. 2a shows the frequency dependence of loss tangent of samples with a silver electrode, demonstrating that the loss tangents are much lower than those of the samples with the same composition but with an aluminium electrode. Maxima occur in the loss tangent curves. The equivalent circuit of specimens can be depicted as a series of three RC sections as shown in Fig. 3. An individual section represents the part coming from the grains, boundary layers, and electrodes, respectively. The grain and boundary layer sections can be combined as a $R_m C_m$ section, indicating material section. The measured equivalent resistivities of whole specimens are presented in Figs 1b and 2b, showing that the resistivities of samples with silver electrodes are 3 to 4 orders of magnitude higher than those with aluminium electrodes. The evaporated aluminium electrode is found to be an ohmic contact, therefore the measured resistivities of samples with aluminium electrodes should be essentially R_m. The silver electrode prepared from silver paste blocks charge carriers, the measured resistivities mainly result from the interfacial layer between the silver electrode and the ceramics, i.e. R_{el}. The effective material resistivity R_m decreases with an increasing amount of barium dopant. This is contrary to what is expected from the viewpoint that barium traps two electrons when it is dissolved into a titanium lattice site, i.e. Ba_{Ti}. The order of R_m lies in a range corresponding to that of n-type semiconducting TiO_2. Fig. 1c shows the frequency dependence of the relative dielectric constant for samples with an aluminium electrode, illustrating very high relative dielectric constants with an order of about 10^5–10^6. The capacitances of samples with aluminium electrodes are found to decrease with increasing d.c. bias voltage. A plot of $(1/C-1/2C_0)^2$ against V shows a linear relationship which is compatible with the symmetric back-to-back Schottky barrier model, where C_0 is the capacitance measured at zero d.c. bias voltage, and C is the capacitance measured at d.c. bias voltage V. These results show that there are space charge regions near boundary layers which are very likely to be caused by boundary segregation of barium, however, the space charge regions are not very effective in preventing charge carriers from crossing. Fig. 2c shows the frequency dependence of the relative dielectric constant for samples with a silver electrode. Since the silver electrode forms a block layer, C_{el} can not be ignored. The resultant capacitance is essentially determined by the smaller one between C_m and C_{el} if they differ from each other greatly. From a comparison of Figs 1c and 2c, it is obvious that C_{el} is much smaller than C_m in the case of the silver electrode. From Figs 2b and c it can be seen that the silver-electroded samples possess ultrahigh relative dielectric constants with an order of about 10^5 and relatively low loss tangents, about 4% for some samples. The following discussion will be concentrated on silver-electroded samples due to their excellent dielectric properties.

4.2. Migration mechanism of barium and niobium doped TiO_2 ceramics

By plotting an Arrhenius diagram of ln (f_r) against $1/T$, and applying Equation 2 the activation energies of the migration mechanism for samples of different compositions as well as different sintering and annealing conditions were obtained and listed in Table III. The linear relationships of ln (f_r) against $1/T$ for all samples are excellent in the measuring temperature range, i.e. −20–100° C, for all samples. From Table III, the observed activation energies vary from 0.16 to 0.20 eV, with an average value at 0.18 eV. The

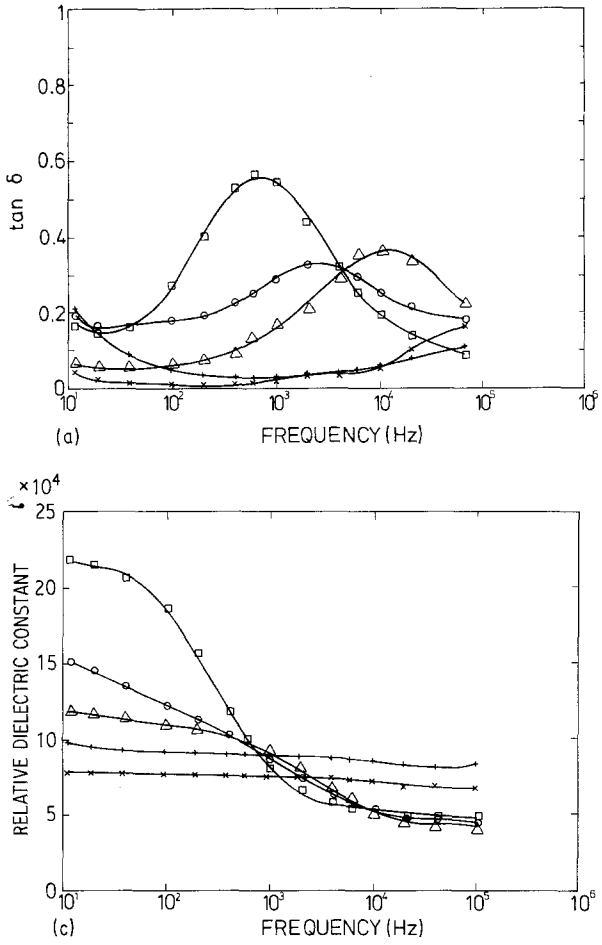

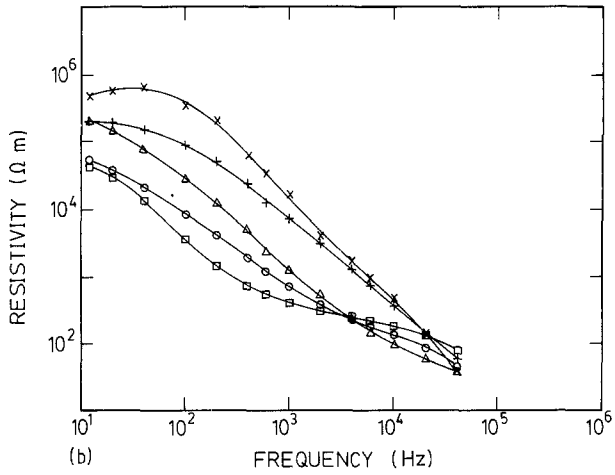

Figure 2 Frequency dependence of (a) tan δ, (b) resistivity, and (c) relative dielectric constant for samples with silver electrode. Symbols as for Fig. 1.

activation energies for 25IN100IB and 25IN120IB compositions are not shown in Table III because there were no peaks observed in the measuring frequency (10–10^5 Hz) and temperature ranges (-25–100°C). As for the 25IN80IB composition under T1A2 sintering and annealing conditions, the peaks were broad and the maxima were not clear, the locations of relaxation frequencies were very difficult to determine, hence the activation energy was not included in Table III either.

By summarizing the temperature and oxygen pressure dependence of electrical conductivity and other defect-dependent properties [5–8], Kofstad [9] proposed that the defect structure of TiO_2 ceramics simultaneously comprises doubly charged oxygen vacancies and interstitial titanium ions with three and four effective charges. His model predicted that oxygen vacancies predominate at near atmospheric oxygen pressures.

TABLE III Activation energies of migration mechanism for samples with different compositions and firing conditions

Firing condition		*T*1	*T*1A1	*T*1A2	*T*1A3
Sintering temperature for 2 h	1450° C	1350° C	1350° C	1350° C	1350° C
Annealing temperature after sintering for 6 h	No	No	1050° C	850° C	700° C
25IN	0.19				
25IN20IB		0.17	0.20	0.20	0.17
25IN80IB		0.17	0.16	?	0.18
25IN100IB		?	?	?	?
25IN120IB		?	?	?	?
100IN80IB		0.20	0.19	0.19	0.19

The unit of activation energy is eV.

Breckenridge and Hosler [10] studied the electrical properties of TiO_2 semiconductors under various preparation conditions and concluded that there are three types of oxygen vacancy defects present. The oxygen vacancy has an effective charge of $+2$, and Ti'_{Ti} where one electron locates has an effective charge of -1, thus it is possible to have present in the crystal neutral centres ($V_O^{\cdot\cdot} \cdot 2Ti'_{Ti}$), single ionized centres ($V_O^{\cdot\cdot} \cdot Ti'_{Ti}$)$^{\cdot}$ and free oxygen vacancies $V_O^{\cdot\cdot}$. From conductivity studies, two types of donor centres were suggested: the neutral centres being those with a small activation energy for ionization, 0.01 eV, and the singly ionized centres with the larger energy, 0.20 eV. There may also be present a considerable number of free oxygen vacancies, produced along with a corresponding number of vacant Ti^{4+} sites as normal Schottky defects. An energy-level diagram of semiconducting rutile shown in Fig. 4 was proposed by Breckenridge and Hosler [10] to explain the conductivity properties of TiO_2 ceramics.

Since the activation energy of the migration mechanism observed in the present study, ranging from 0.16 to 0.2 eV with an average at 0.18 eV, is very close to 0.20 eV, it is proposed that the migration mechanism of barium and niobium doped TiO_2 ceramics involve hopping of electrons from singly ionized centres

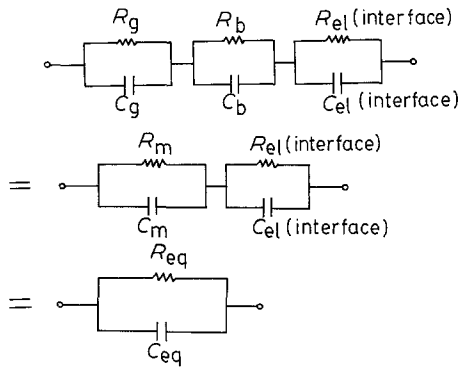

Figure 3 Equivalent circuits of specimens.

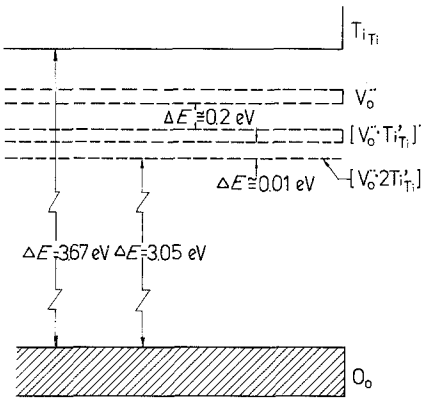

Figure 4 Energy-level diagram of rutile (TiO_2), after [10].

$(V_O^{\cdot\cdot} \cdot Ti'_{Ti})^{\cdot}$ to free oxygen vacancies $V_O^{\cdot\cdot}$. It is reasonable to suggest that the magnitude of electrical conductivity is closely related to the probability of electron hopping between singly ionized centres and free oxygen vacancies. As the concentration of free oxygen vacancy increases, the average distance between the free oxygen vacancy and singly ionized centre decreases, hence the probability of electron hopping increases and results in an increase of electrical conductivity. Similarly, the increase of the concentration of Ti'_{Ti}, i.e. electron, provides more electrons available to hop and hence affects the electrical conductivity.

4.3. The effect of barium dopant

The relaxation frequency of loss tangent for samples with a silver electrode is shown in Fig. 2a. There are no peaks observed for compositions 25IN100IB and 25IN120IB. However, by decreasing the measuring temperature, peaks start to appear in the high frequency end, i.e. 10^5 Hz. This means that the relaxation frequencies of these two compositions are higher than 10^5 Hz as measurement is carried out at room temperature. The relaxation frequency increases with the amount of barium dopant for all compositions investigated. According to Equation 2, the relaxation frequency increases with the conductivity of the ceramics, which is compatible with what is observed in Fig. 1b. The effect of barium can be interpreted by defect Equation 3.

$$BaO \rightleftharpoons Ba''_{Ti} + V_O^{\cdot\cdot} + O_O \qquad (3)$$

As barium is dissolved into TiO_2 one free oxygen vacancy is created. In the extrinsic region the concentration of free oxygen vacancies is almost fixed by the concentration of dissolved barium. The increase in oxygen vacancy concentration enhances the electron hopping probability and results in an increase of conductivity. Since $R_{el} > R_m$ and $C_{el} < C_m$, the relative dielectric constant and resistivity of samples with a silver electrode depend greatly on the interfaces between the silver electrode and the ceramics. The resistivity and the width of the interfacial layer determine the resistivity and relative dielectric constant of the sample, especially in the low frequency region. Fig. 2b shows that the resistivity of the sample increases with the amount of barium in the low frequency region; on the other hand, the resistivity of the sample tends

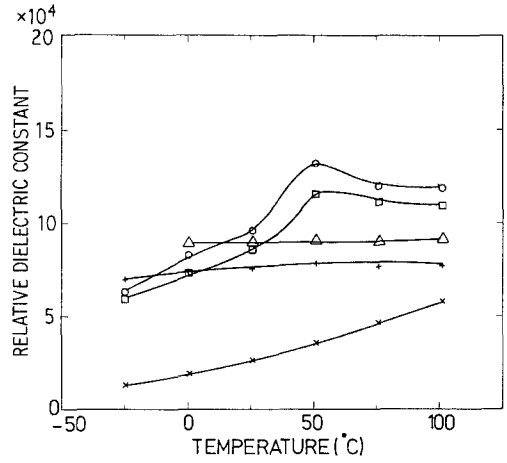

Figure 5 Temperature dependence of relative dielectric constant measured at 1 kHz for samples with silver electrode. (□ 25IN20IB, ○ 25IN80IB, △ 25IN100IB, + 25IN120IB, × 100IN80IB).

to decrease with the amount of barium in the high frequency region. Fig. 2c illustrates that the relative dielectric constant decreases abruptly with frequency for samples doped with barium less than 0.80 mol %; in contrast, the relative dielectric constant remains virtually constant with the variation of frequency for samples doped with barium more than 1.00 mol %. According to theoretical analysis [1, 3, 4], the relative dielectric constant is expected to change rapidly near the relaxation frequency. The higher the amount of barium dopant, the higher the relaxation frequency, and hence the less variation of relative dielectric constant in the measured frequency range. The properties measured in the low frequency region rely strongly on the characteristics of the high resistivity interface and those measured in the high frequency region virtually reflect the properties of the low resistivity ceramics. The effects of barium on resistivities and relative dielectric constants of silver-electroded samples can be interpreted if it is assumed that the thickness of the interfacial layer is larger for samples doped with a higher amount of barium. A thicker interfacial layer resulted in higher resistivity and lower relative dielectric

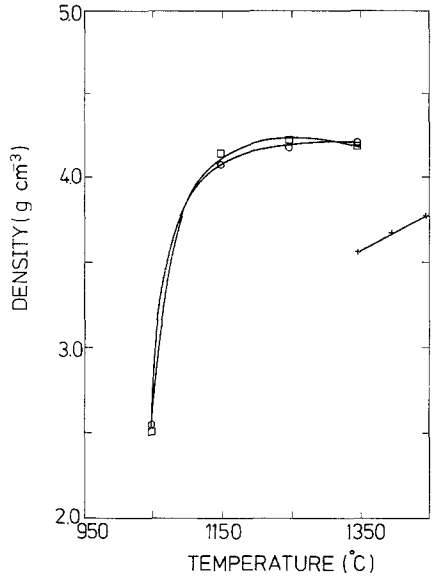

Figure 6 Sintered bulk density against sintering temperature after 2 h sintering (□ 100IN80IB, ○ 25IN80IB, + 25IN).

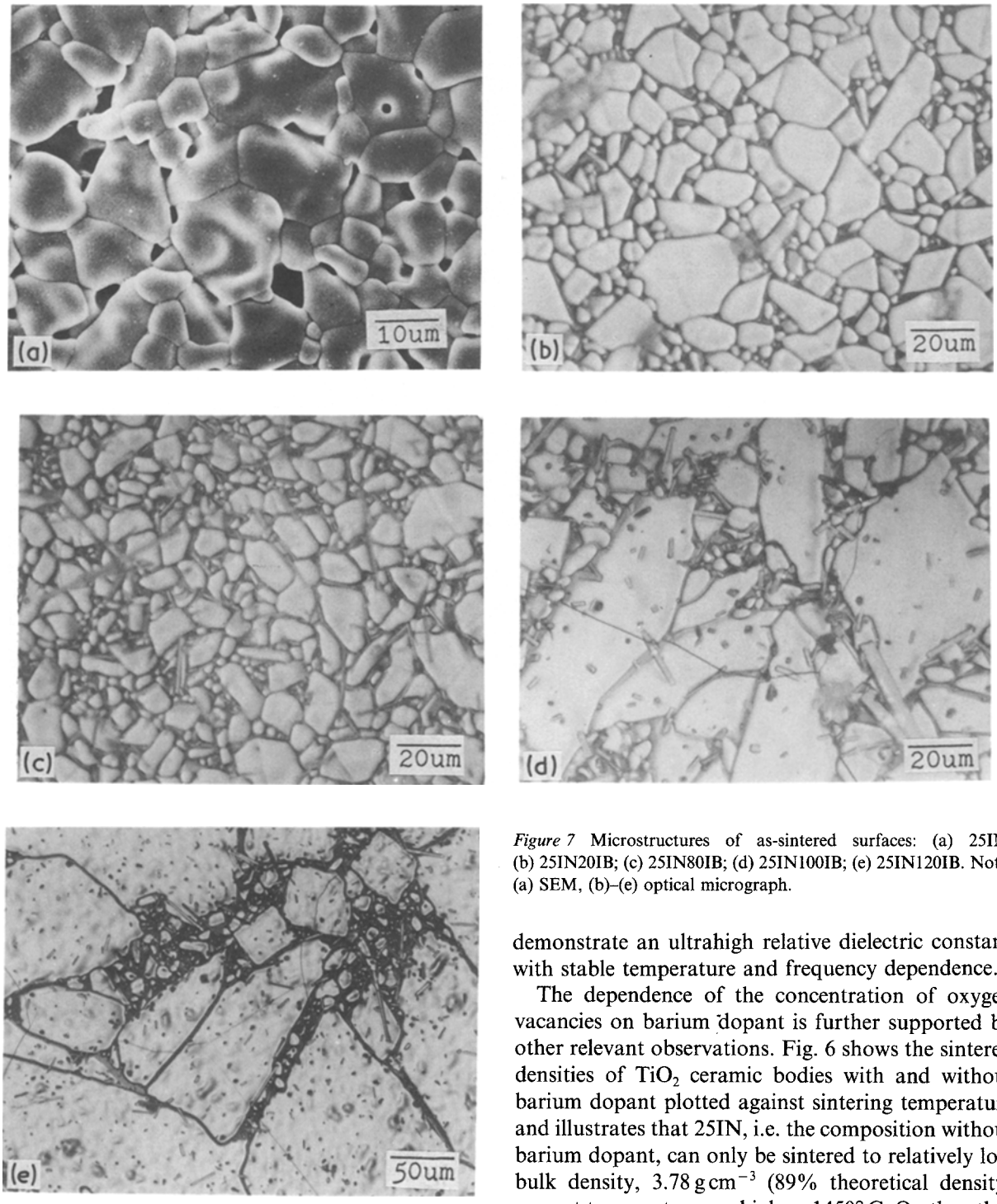

Figure 7 Microstructures of as-sintered surfaces: (a) 25IN; (b) 25IN20IB; (c) 25IN80IB; (d) 25IN100IB; (e) 25IN120IB. Note: (a) SEM, (b)–(e) optical micrograph.

constant in the low frequency region. This is consistent with the observations. Since the relaxation frequency changes with the measuring temperature, the variation of relative dielectric constant with frequency changes simultaneously. Fig. 5 presents the temperature dependence of the relative dielectric constant measured at 1 kHz, illustrating that the relative dielectric constant remains almost unchanged with temperature for compositions 25IN100IB and 25IN120IB. This is because the relaxation frequency is generally higher than 10^5 Hz in the measuring temperature range, no variation of relative dielectric constant with frequency is observed. The relative dielectric constant is only dependent on the thickness of the interfacial layer which will not change with the measuring temperature. Compositions 25IN100IB and 25IN120IB demonstrate an ultrahigh relative dielectric constant with stable temperature and frequency dependence.

The dependence of the concentration of oxygen vacancies on barium dopant is further supported by other relevant observations. Fig. 6 shows the sintered densities of TiO_2 ceramic bodies with and without barium dopant plotted against sintering temperature and illustrates that 25IN, i.e. the composition without barium dopant, can only be sintered to relatively low bulk density, 3.78 g cm^{-3} (89% theoretical density) even at temperatures as high as 1450° C. On the other hand, the 25IN80IB composition can be sintered to about 4.20 g cm^{-3} (99% theoretical density) in the temperature range from 1150 to 1350° C. Barringer *et al.* [11] proposed in a sintering study of monodisperse TiO_2 that oxygen diffusion, which depends on the concentration of oxygen vacancy, is the major factor that determines the sintering kinetics. The conclusion that oxygen vacancies are rate controlling in sintering TiO_2 is also obtained by Anderson [12]. The observations shown in Fig. 7 demonstrate the enhancement of sintering as a result of barium dopant in TiO_2 ceramics. Barringer's conclusion supports the argument that the concentration of oxygen vacancies increases with increasing barium dopant.

Fig. 7 shows the microstructures of as-sintered surfaces of compositions with different amount of barium dopant, illustrating that there is a tendency of abnormal

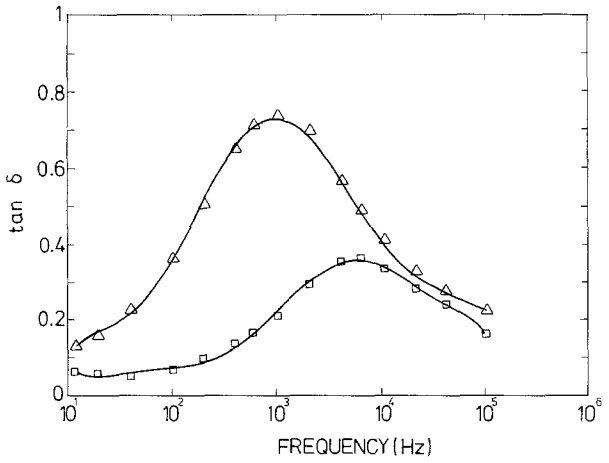

Figure 8 Frequency dependence of tan δ for compositions with different amount of niobium (silver electrode) (□ 25IN80IB, △ 100IN80IB).

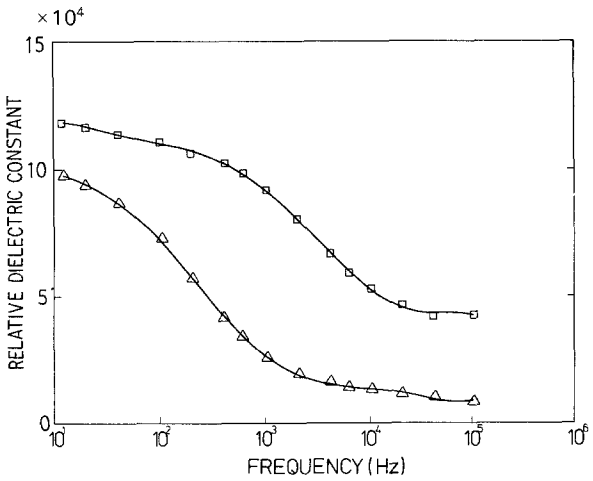

Figure 9 Frequency dependence of relative dielectric constant for compositions with different amount of niobium (silver electrode) (□ 25IN80IB, △ 100IN80IB).

grain growth as the amount of barium dopant increases. From X-ray diffraction analysis, all samples doped with barium contain a small amount of second phases like $BaTi_4O_9$, $Ba_2Ti_9O_{20}$, and some unidentified phases. Although, the amounts of second phases roughly increase with the amount of barium dopant as results of X-ray diffraction analysis and microstructural observations, it is believed that the amount of barium dissolved in the TiO_2 matrix is still higher for higher barium dopant. When ceramic powders are very fine, the presence of second phases is very likely to trigger abnormal grain growth if the diffusion coefficient, especially of oxygen, is high. The oxygen diffusion coefficient mainly depends on the concentration of oxygen vacancies. All observations agree very well with the argument that the addition of barium increases the concentration of oxygen vacancies and causes the increase of relaxation frequency of loss tangent.

4.4. The effect of niobium dopant

Fig. 8 shows the effect of niobium dopant on the frequency dependence of loss tangent measured at room temperature for samples with a silver electrode, illustrating that the relaxation frequency decreases with increasing amount of niobium dopant. The effect of niobium dopant can be explained by defect Equations 4 and 5

$$Nb_2O_5 \rightleftharpoons 2Nb_{Ti}^{\cdot} + 2e' + 4O_0 + \tfrac{1}{2}O_2(g) \quad (4)$$

$$2TiO_2 \rightleftharpoons 2Ti_{Ti}' + V_0^{\cdot\cdot} + 3O_0 + \tfrac{1}{2}O_2(g) \quad (5)$$

where the electron usually combines with the regular titanium lattice ion and forms Ti_{Ti}'. The dissolution of niobium into TiO_2 ceramics increases the concentration of e′, which is equivalent to Ti_{Ti}', and the local oxygen partial pressure according to Equation 4, these in turn tend to decrease the concentration of oxygen vacancies according to Equation 5. Hence the resultant relaxation frequency decreases with the amount of niobium dopant. Fig. 9 shows the frequency dependence of the relative dielectric constant for the silver-electroded samples with different amounts of niobium. As discussed in the previous section, the relative dielectric constant depends on the interfacial characteristics and relaxation frequency. The relative dielectric constant is found to decrease with the amount of niobium dopant in the low frequency region.

Fig. 10 illustrates the microstructures of as-sintered surfaces of compositions with different niobium content. As it can be seen in Fig. 10, the degree of abnormal grain growth is much higher for samples doped with lower niobium content. The grain size of the composition doped with 1.00 mol % niobium is relatively uniform. This characteristic is consistent with the argument that the oxygen vacancy concentration decreases with increasing niobium content.

5. Conclusion

The migration mechanism proposed is electron hopping among oxygen vacancies. The conductivity increases with the concentration of oxygen vacancies because of an increased probability of electron hopping. The boundary space charge region is found to exist in barium and niobium doped TiO_2 ceramics, however, the boundary layer is not effective in stopping electron crossing. An evaporated aluminium electrode forms ohmic contact on barium and niobium doped TiO_2 ceramics and thus samples with an evaporated aluminium electrode behave like lossy capacitors especially in the low frequency region. The silver electrode made from silver paste forms non-ohmic contact on barium and niobium doped TiO_2 ceramics and blocks electrons. The frequency dependence of the relative dielectric constant depends greatly on the relaxation frequency of the loss tangent which increases with conductivity of the ceramics.

Barium dopant, when dissolving into TiO_2 ceramics, increases the concentration of oxygen vacancies which in turn increases the relaxation frequency. Compositions doped with 0.25 mol % Nb and 1.0 or 1.2 mol % Ba show stable frequency and temperature dependence of relative dielectric constant because of their relatively high relaxation frequency. These two compositions also possess ultrahigh relative dielectric constants of about 10^5 and low loss tangents of about 4%. In contrast, niobium dopant decreases the concentration of oxygen vacancies, and thus results in a lower relaxation frequency.

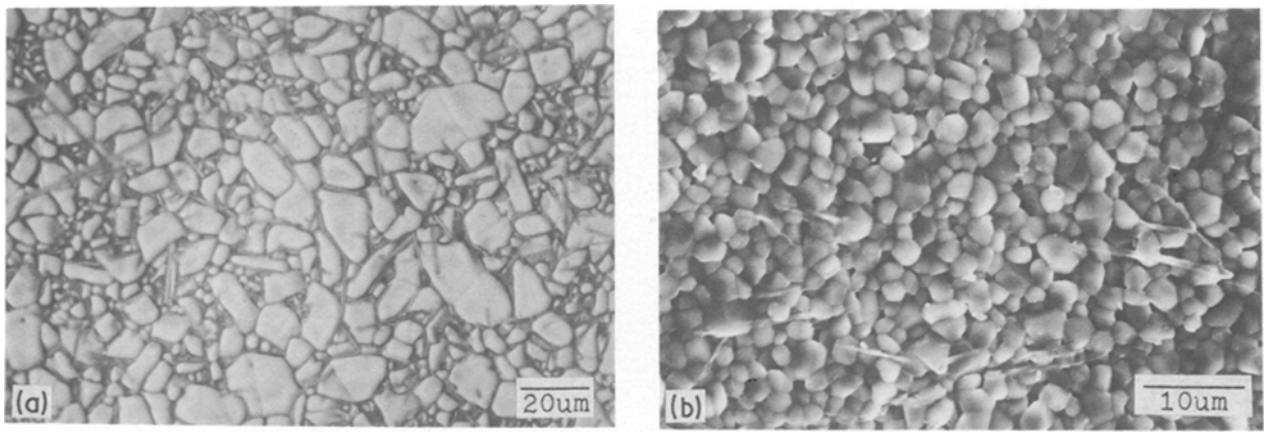

Figure 10 Microstructures of as-sintered surfaces: (a) 25IN80IB, optical micrograph, and (b) 100IN80IB, SEM.

References

1. C. G. KOOPS, *Phys. Rev.* **83** (1951) 121.
2. M. F. YAN and W. W. RHODES, "Advances in Ceramics", Vol. 7, edited by M. F. Yan and A. H. Heuer (The American Ceramic Society, Columbus, Ohio, 1983) p. 226.
3. J. C. MAXWELL, in "Electricity and Magnetism," Vol. 1 (Clarendon, Oxford, 1892).
4. K. W. WAGNER, *Arch. Electrotechnik* **2** (1914) 371.
5. P. KOFSTAD, *J. Phys. Chem. Solids* **23** (1962) 1579.
6. K. S. FØRLAND, *Acta Chem. Scand.* **18** (1964) 1267.
7. J. B. MOSER, R. N. BLUMENTHAL and D. H. WHITMORE, *J. Amer. Ceram. Soc.* **48** (1965) 384.
8. C. B. ALCOCK, S. ZADOR and B. C. H. STEELE, *Proc. Brit. Ceram. Soc.* **8** (1967) 231.
9. P. KOFSTAD, *J. Less-Common Met.* **13** (1967) 635.
10. R. G. BRECKENRIDGE and W. R. HOSLER, *Phys. Rev.* **91** (1953) 793.
11. E. A. BARRINGER, R. BROOK and H. K. BOWEN, in "Materials Science Research", Vol. 16, edited by G. C. Kuczynski, A. E. Miller and G. A. Sargent (Plenum Press, New York, 1984) p. 1.
12. H. U. ANDERSON, *J. Amer. Ceram. Soc.* **50** (1967) 235.

Received 9 December 1987
and accepted 29 April 1988